

Hydroxyapatite coating on magnesium with MgF₂ interlayer for enhanced corrosion resistance and biocompatibility

Ji-Hoon Jo · Bong-Gyu Kang · Kwang-Seon Shin ·
Hyoum-Ee Kim · Byung-Dong Hahn ·
Dong-Soo Park · Young-Hag Koh

Received: 18 October 2010 / Accepted: 25 August 2011 / Published online: 10 September 2011
© Springer Science+Business Media, LLC 2011

Abstract Hydroxyapatite (HA) was coated onto pure magnesium (Mg) with an MgF₂ interlayer in order to reduce the surface corrosion rate and enhance the biocompatibility. Both MgF₂ and HA were successfully coated in sequence with good adhesion properties using the fluoride conversion coating and aerosol deposition techniques, respectively. In a simulated body fluid (SBF), the double layer coating remarkably enhanced the corrosion resistance of the coated Mg specimen. The *in vitro* cellular responses of the MC3T3-E1 pre-osteoblasts were examined using a cell proliferation assay and an alkaline phosphatase (ALP) assay, and these results demonstrated that the double coating layer also enhanced cell proliferation and differentiation levels. In the *in vivo* study, the HA/MgF₂ coated Mg corroded less than the bare Mg and had a higher bone-to-implant contact (BIC) ratio in the cortical bone area of the rabbit femora 4 weeks after implantation. These *in vitro* and *in vivo* results suggested that the HA coated Mg with the MgF₂ interlayer could be used as a potential candidate for biodegradable implant materials.

1 Introduction

Degradable biomaterials that can be absorbed in the body are considered a new paradigm of materials for biomedical applications [1]. The introduction of biodegradable implants eliminates the typical problems that are associated with permanent implants, such as stress shielding, the accumulation of toxic metal ions, and the need for a second surgery in order to remove the implant. Synthetic biodegradable polymers, including poly lactic acid (PLA), poly glycolic acid (PGA) and poly caprolactone (PCL), have widely been used as substitutes for permanent implants in orthopedic applications [2]. However, these polymeric materials have lower mechanical strengths than metallic materials and are more suitable for low load-bearing applications [3].

Recently, magnesium (Mg) and its alloys have been considered as promising degradable biomaterials because of their advantages over synthetic polymers, especially in terms of their mechanical properties. The elastic modulus and the compressive strength of Mg are relatively close to the values for natural bones and are much better than other implantable metals. Additionally, Mg has a higher fracture toughness than natural bone [4]. Therefore, Mg and its alloys could potentially be used for load-bearing applications. Moreover, previous studies have demonstrated that Mg has a good biocompatibility, and any released Mg ions are not detrimental to the human body but rather beneficial to the bone tissue growth [4, 5]. Nevertheless, the use of Mg in biomedical applications has been restricted mainly because of its high and unpredictable corrosion rate in biological ambience. The Mg surface rapidly reacts with aqueous solutions, generating by-products, such as hydroxide ions and hydrogen gas. [6] Additionally, these Mg corrosion reactions are accelerated in chloride-containing solutions (e.g. human body fluid, blood plasma) [7]. If the

J.-H. Jo · B.-G. Kang · K.-S. Shin · H.-E. Kim (✉)
WCU Hybrid Materials Program, Department of Materials
Science and Engineering, Seoul National University,
Seoul 151-744, Korea
e-mail: kimhe@snu.ac.kr

B.-D. Hahn · D.-S. Park
Functional Ceramics Group, Functional Materials Division,
Korea Institute of Materials Science (KIMS), Changwon,
Gyeong-Nam 641-010, Republic of Korea

Y.-H. Koh
Department of Dental Laboratory Science and Engineering,
Korea University, Seoul 136-706, Republic of Korea

Mg corrosion is too rapid, the mechanical integrity of the implant can be lost before the tissue has sufficiently healed [4]. Therefore, this corrosion reaction must be suppressed by enhancing the corrosion resistance of the Mg surface in order to maintain the mechanical integrity of the Mg implant.

To date, numerous methods, such as alloying and surface treatments, have been studied in order to improve the corrosion resistance of Mg. In particular, various Mg alloys have been investigated as potential degradable biomaterials, and some of these alloys have exhibited *in vitro* and *in vivo* biocompatibility [8–19]. Additionally, previous reports have shown that some of these alloying elements can strongly influence the corrosion resistance, the strength, and the biocompatibility of Mg [17, 20]. Although many studies have investigated the toxicity of these alloying elements, great care must be taken during the selection of the alloying element as well as the amount that is used, and further investigations are required for safe clinical use.

The implant material could be surface treated to enhance both the corrosion resistance and the biocompatibility. This method has practically been used in metal implants, such as stainless steel, titanium, and titanium alloys. For biomedical applications, various surface treatments have been adopted for Mg and its alloys in order to control the degradation rate and improve the biocompatibility [3, 21–29]. In the literature, the electrochemical and immersion test results have confirmed that surface treatments can significantly reduce the degradation rate of Mg-based materials in chloride-containing solutions. Furthermore, the surface biocompatibility of Mg can also be enhanced using bioactive coatings, such as calcium phosphate coatings [26–28, 30]. Among them, hydroxyapatite (HA) coatings are well recognized because of their excellent bioactivity, which improves the bonding between the metal implant and the bone [31, 32].

In this present work, HA was coated onto pure Mg with an MgF₂ interlayer in order to control and predict the degradation rate and at the same time to improve the surface bioactivity of Mg. The MgF₂ layer was formed on Mg as a corrosion barrier prior to the HA coating [3]. Then HA was deposited onto the MgF₂-coated Mg using the aerosol deposition (AD) method. This method created a dense ceramic layer from the starting ceramic particles at room temperature without any additional heat treatment [33]. The initial corrosion properties of the bare and coated Mg were evaluated in a simulated body fluid (SBF). The *in vitro* cell tests were performed using pre-osteoblasts in order to observe the cellular responses on the bare and coated Mg, and the animal tests were implemented in order to assess the *in vivo* interaction between the Mg implant and the bone tissue.

2 Materials and methods

2.1 Sample preparation and coating procedure

The Mg samples were prepared with dimensions of 20 mm × 20 mm × 3 mm using a commercial pure magnesium ingot (purity 99.99%, Yi Riu Magnesium Ind., Co, Beijing, China). Rod samples, with a diameter of 4 mm and a length of 10 mm, were used for the *in vivo* studies. Prior to the coating process, the Mg samples were polished with up to 2000 grit abrasive paper and ultrasonically cleaned in acetone and ethanol.

For the MgF₂ coating process, the Mg samples were immersed in hydrofluoric acid (48 wt% in H₂O, Sigma-Aldrich, USA) at room temperature for 24 h. The coated samples were rinsed with both distilled water and ethanol and then dried in air. Subsequently, hydroxyapatite (HA) was coated onto the fluoride-coated Mg samples using the aerosol deposition (AD) method. For the AD process, commercially available nanocrystalline HA (Alfa Aesar Co., Ward Hill, MA) was used as the starting powder, and the HA coating was deposited at a thickness of 5 μm. The coating apparatus and process conditions were described in detail in the literature [34]. In brief, the HA powder heat-treated at 1200°C for 1 h was loaded in the powder chamber and sprayed into the deposition chamber using an oxygen carrier gas at a flow rate of 5×10^{-4} m³/s. During deposition, the HA particles were vertically sprayed onto the substrate and the pressure in the deposition chamber was 0.92×10^{-3} MPa.

2.2 Characterization

The surface morphology and the chemical composition of the samples were analyzed using scanning electron microscopy (SEM, JSM-6360, JEOL, Tokyo, Japan) with an EDS system with resolution of 137 eV (INCA system, Oxford Instruments, UK). The cross-sectional morphology of the coated samples was observed using field-emission scanning electron microscopy (FE-SEM, JSM-6330F, JEOL, Tokyo, Japan). The surface phase of the coated samples was characterized using an X-ray diffractometer (XRD, D8-Advance, Bruker Co., Germany). The XRD data were obtained from 20° to 60° (2θ) using CuK_α radiation with a scan rate of 1°/min. The sample measurement area was 20 mm × 20 mm. The adhesion strength of the coating layers was measured using an adhesion tester (Sebastian V, Quad Group, Spokane, WA, USA). Prior to the adhesion test, a pre-epoxy coated stud with a diameter of 3.58 mm was attached to the coating surface and cured at 150°C for 1 h in an oven. After the tester jig was fixed to the sample, the stud was pulled in the vertical direction until the coating layer failed. The adhesion strength was

calculated using the maximum recorded tensile force values and the failure area. Five coated samples were tested for each coating condition, and the average value was used.

2.3 Immersion tests

The immersion tests were carried out in the SBF for up to 3 days in order to evaluate the initial surface corrosion properties of the samples [35]. The samples were immersed in 100 ml of the SBF with an exposure area of 2 cm² at room temperature. pH measurements were done about 2 cm above the sample after stirring sufficiently. After each immersion period, 5 ml of the solution was extracted and analyzed using an inductively-coupled plasma atomic-emission spectrometer (ICP-AES, Optima-4300DV, PerkinElmer, Wellesley, MA) in order to determine the magnesium ion concentration. The pH value of the immersion solution was also monitored at different time intervals using a pH meter (sp-701, Suntext, Taiwan). Three samples were tested at each condition for the immersion tests.

2.4 In vitro cell tests

A pre-osteoblast cell line, MC3T3-E1 (ATCC, CRL-2593), was used to assess the cellular responses on the specimen surfaces. Prior to the cell seeding, the samples were sterilized with 70% ethanol and dried on a clean bench under UV irradiation. The pre-incubated cells were seeded on the specimens with a diameter of 15 mm at densities of 5×10^4 cells/ml (for the cell attachment), 3×10^4 cells/ml (for the cell proliferation), and 1.5×10^4 cells/ml (for the cell differentiation). The cells were cultured in a medium, consisting of an alpha-minimum essential medium (α -MEM, Welgene Co., Ltd., Korea) that was supplemented with 5% fetal bovine serum (FBS) and 1% penicillin–streptomycin in a humidified incubator with 5% CO₂ at 37°C.

The attached cells were observed using scanning electron microscopy (SEM, JSM-5600, JEOL, Tokyo, Japan) after culturing for 5 h and 1 day. Prior to these observations, the samples were fixed with 2.5% glutaraldehyde for 10 min, dehydrated in graded ethanol (70, 90, 95 and 100% ethanol in sequence), immersed in hexamethyldisilazane for 10 min, and then air dried. The DNA from the samples was examined using a Cyquant cell proliferation assay kit (C7026 Invitrogen) after culturing for 1 day. The cells that adhered to the samples were detached and suspended in a fluorescent dye solution. The DNA level was measured using a multiple plate reader (Victor3, PerkinElmer, USA) at a wavelength of 480/535 nm. The measured fluorescence values were converted into the DNA content using a DNA standard curve. Additionally, the cell proliferation on the specimens was assessed for up to 4 day using this cell proliferation assay kit.

To evaluate the cell differentiation, 10 mM β -GP and 50 μ g/ml ascorbic acid were added to the culture medium, and an alkaline phosphatase (ALP) activity test was performed using *p*-nitrophenyl phosphate (pNPP, Sigma-Aldrich, UK). After culturing for 10 days, the *p*-nitrophenol (pNP) production was colorimetrically measured at an absorbance of 405 nm using a micro reader (Biorad, Model 550, USA). During this reaction, pNPP was converted into pNP in the presence of ALP, and therefore, the pNP production rate was proportional to the ALP activity.

In vitro cell tests were performed at least three times, and the experimental results were expressed as the mean \pm standard deviation (SD). The difference between the two groups was determined using a one-way analysis of variance (ANOVA), and a $P < 0.05$ was considered statistically significant.

2.5 In vivo animal tests

The in vivo animal tests were conducted using nine male New Zealand white rabbits (12 weeks old, average weight 3 kg). Two types of rod samples (bare Mg and HA/MgF₂ coated Mg) with diameters of 4 mm and lengths of 10 mm were used in this study. The animals were given a general anesthetic using a combination of 1.5 cc of 2% Xylazine HCl (Rompun, Bayer Korea, Korea) and 0.5 cc of Tiletamine HCl (Zoletil, Virbac lab, France) and Lidocaine (Yuhan Corporation, Korea). Additionally, 1:100,000 epinephrine was injected as the local anesthesia. The rod samples were implanted into femoral defects on either the left or right leg of the rabbits that drilled into the femoral shaft using a hand piece drill. After the surgery, the wounds were sutured with Surgisorb (Samyang Ltd, Korea), and then cephadrine (Bayer Korea, Korea), an antibiotic, was injected into the rabbits for 3 days.

All of the rabbits were sacrificed 4 weeks after surgery. The harvested bone tissues were scanned using a micro-CT (Skyscan 1173 X-ray Micro-tomography System, Skyscan, Kontich, Belgium) with a 1.0 mm aluminum filter at a resolution of 35 μ m, a voltage of 100 kV, and a current of 60 μ A in order to 3-dimensionally observe the morphology of the Mg samples and the bone tissue. Subsequently, the images were reconstructed using a commercial program, and the implant morphology and the bone tissue in the cortical area were 3-dimensionally observed using Data viewer (Skyscan, Kontich, Belgium) based on these reconstructed images.

After the micro-CT scan, the extracted bone samples were fixed in a neutral 10% formaldehyde solution, and the tissue blocks were formed using a resin. The blocks were cut into sections around cortical bone region. The microscopic images of the trichrome and haematoxylin–eosin stained sections were obtained using Axioskop microscopy (Olympus BX51,

Olympus Corporation, Tokyo, Japan) at a 100 \times magnification. The bone-to-implant contact (BIC) ratios were calculated from these images using a digital image analysis program (SPOT, Diagnostic instrument, Inc., MI, USA).

3 Results

3.1 Microstructures of MgF₂ and HA coating layers

The surface morphologies of the bare and coated Mg samples are shown in Fig. 1a–d. In Fig. 1a, the bare Mg surface exhibited grooves that were caused by the mechanical grinding. The formation of the MgF₂ layer through fluoridation in an HF solution did not significantly change the morphology because the MgF₂ layer was very thin ($\sim 1.3 \mu\text{m}$), in Fig. 1b. On the other hand, the HA coating layer exhibited a rough surface morphology, in Fig. 1c. At a higher magnification, Fig. 1d confirmed that the rough surface resulted from the presence of micro-scale craters, not pores.

In Fig. 2a, the cross-sectional image revealed that the HA layer was uniform without any observable defects. The thickness of the HA layer was about 5 μm , and the dense MgF₂ interlayer was about 1 μm thick. The HA coating was deposited through aerosol deposition and was well adhered to the MgF₂ barrier coating without any delamination or cracking. In Fig. 2b, the EDS results indicated that the HA coating layer was mainly comprised of Ca, P, and O.

The XRD patterns of the bare Mg and the MgF₂ and HA coating layers are illustrated in Fig. 3. For both coating layer, the crystalline MgF₂ or HA peaks were detected without the presence of any other phase, indicating that the crystalline coating layers were formed without the need for any post treatment that could be detrimental to the highly reactive Mg.

3.2 Adhesion strength of coating layer

The adhesion strengths of the MgF₂ coating on Mg and the HA coating on MgF₂ were measured using the pull-out tests, and the results are presented in Fig. 4. The MgF₂ interlayer that formed as a chemical conversion coating exhibited a strong adhesion to the Mg substrate, with a bonding strength of 34 MPa. The HA coating also exhibited a high bonding strength of 25 MPa, fulfilling the coating material requirements [36]. Interestingly, the bonding strength of HA coating on the MgF₂ (25 MPa) was slightly higher than the HA coating on the bare Mg (22 MPa). Figure 5 shows the surface morphology of the specimen after the HA adhesion test. The adhesion failure occurred between the HA coating and the MgF₂ interlayer as shown in Fig. 5a, even though some of the HA coating (that was detached from the epoxy) was still present along the surface grooves. At a higher magnification, Fig. 5b confirmed that the HA coating was detached from the MgF₂ layer near the adhesion failure.

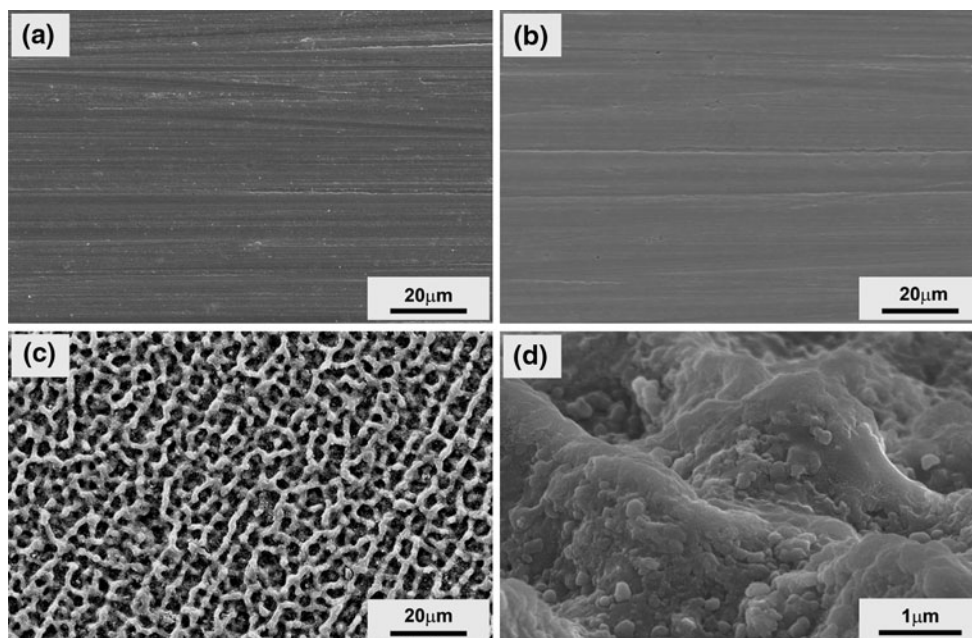


Fig. 1 Scanning electron microscopy (SEM) images of the surfaces of **a** the bare Mg, **b** the MgF₂ coating on Mg, and **c** and **d** the HA coating with the MgF₂ interlayer on Mg

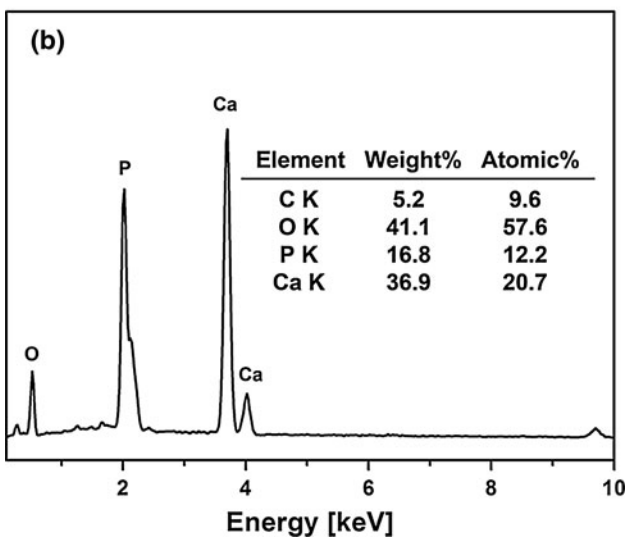
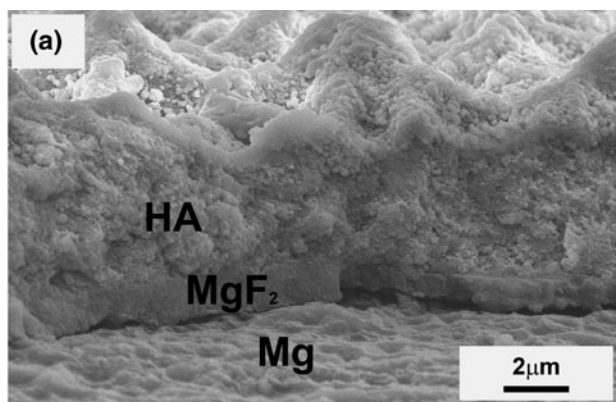


Fig. 2 **a** Cross-sectional image of the HA coating with the MgF₂ interlayer and **b** EDS spectrum of the HA coating layer

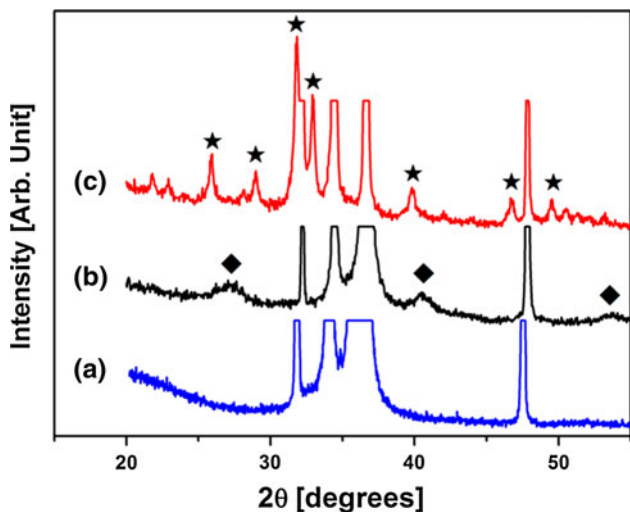


Fig. 3 X-ray diffraction (XRD) patterns of **a** the bare Mg, **b** the MgF₂ coating and **c** the HA coating with the MgF₂ interlayer (filled diamond: MgF₂, filled star: HA)

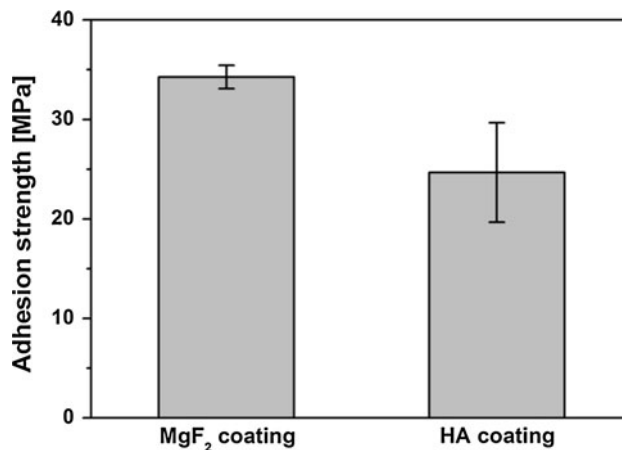


Fig. 4 Adhesion strength of **a** the MgF₂ coating on Mg and **b** the HA coating on MgF₂

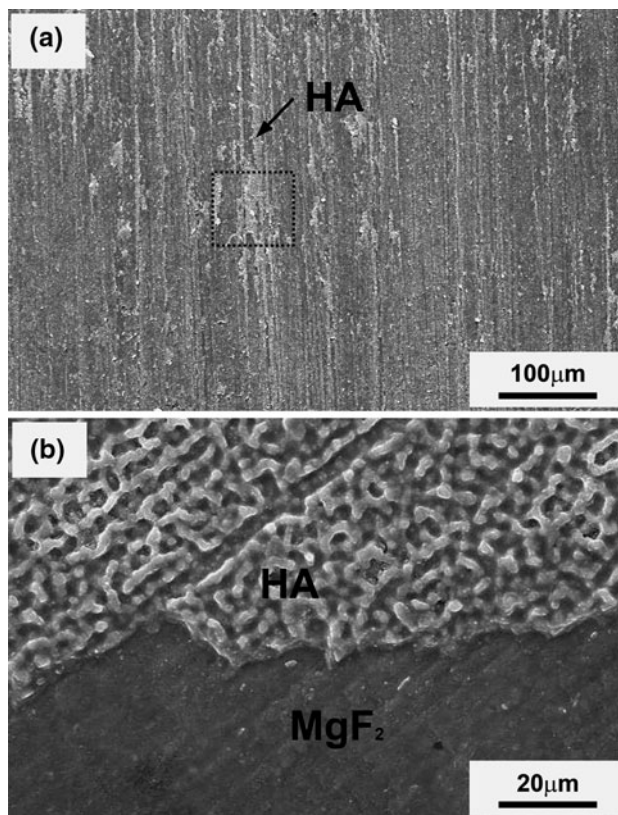


Fig. 5 SEM image of the failure surface for **a** the HA coating on MgF₂ and **b** an enlarged image of the framed area in **a**

3.3 Corrosion properties

The Mg vigorously reacted when the samples were immersed in the SBF solution, resulting in the formation of gas bubbles. On the other hand, the coated samples remained intact for up to 3 days. The released Mg ion concentration

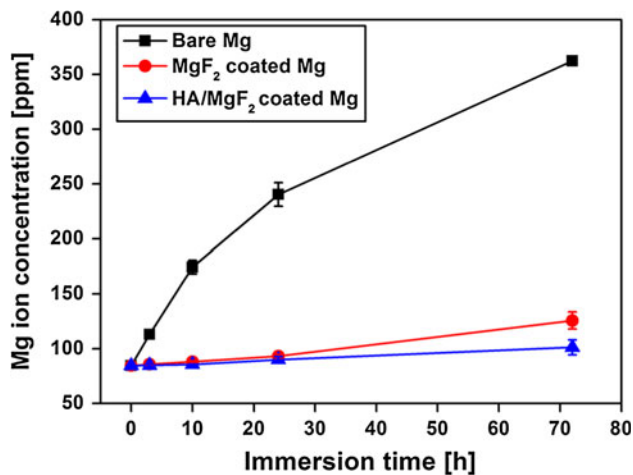


Fig. 6 Released Mg ion concentration in the simulated body fluid (SBF), which was measured using ICP-AES for the bare, MgF₂ coated, and HA/MgF₂ coated Mg samples

and the pH changes in the corrosion media were monitored in Figs. 6 and 7, respectively, in order to evaluate the extent of the Mg corrosion. Less Mg ions were released for the samples with the protective coatings compared to the bare Mg. Additionally, the coating significantly suppressed the pH changes in the SBF compared to the bare Mg. The HA/MgF₂ double coating exhibited a slightly better corrosion resistance than the single MgF₂ coating in the immersion tests. These results indicated that the coating layer protected Mg against corrosion and reduced the alkalization of the medium in the vicinity of Mg.

3.4 In vitro cellular responses

Figure 8 shows the morphology of the pre-osteoblast cells that were cultured for 5 and 24 h on the bare Mg, the Mg that was coated with MgF₂, and the Mg that was coated with MgF₂ and HA. After 5 h, a few spherical cells were attached to the surface of the bare Mg in Fig. 8a. Even after culturing for 24 h, the cells were still in the adhesion stage, and no significant morphology changes were observed, in Fig. 8b. In contrast, clearly, more cells were attached to the MgF₂ surface compared to the bare Mg, in Fig. 8c–d. Furthermore, the cells spread out along the surface, and the extended filopodia reached the surrounding cells, in Fig. 8d. For the HA coated specimens with the MgF₂ interlayer, most of the cells were well attached to the coating surface and spread out after 5 h (Fig. 8e). After culturing for 24 h, the cells were considerably flattened on the rough coating surface, in Fig. 8f. The DNA measurement results are represented in Fig. 8g. The DNA content of the coated samples (both the MgF₂ and HA/MgF₂ coatings) was much greater than the bare Mg, indicating that more cells were attached to the coating surface compared to the bare Mg.

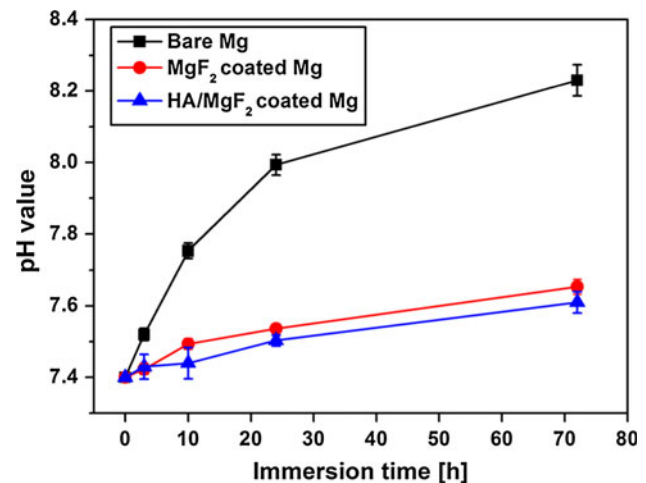


Fig. 7 pH change in the SBF for the bare, MgF₂ coated, and HA/MgF₂ coated Mg samples

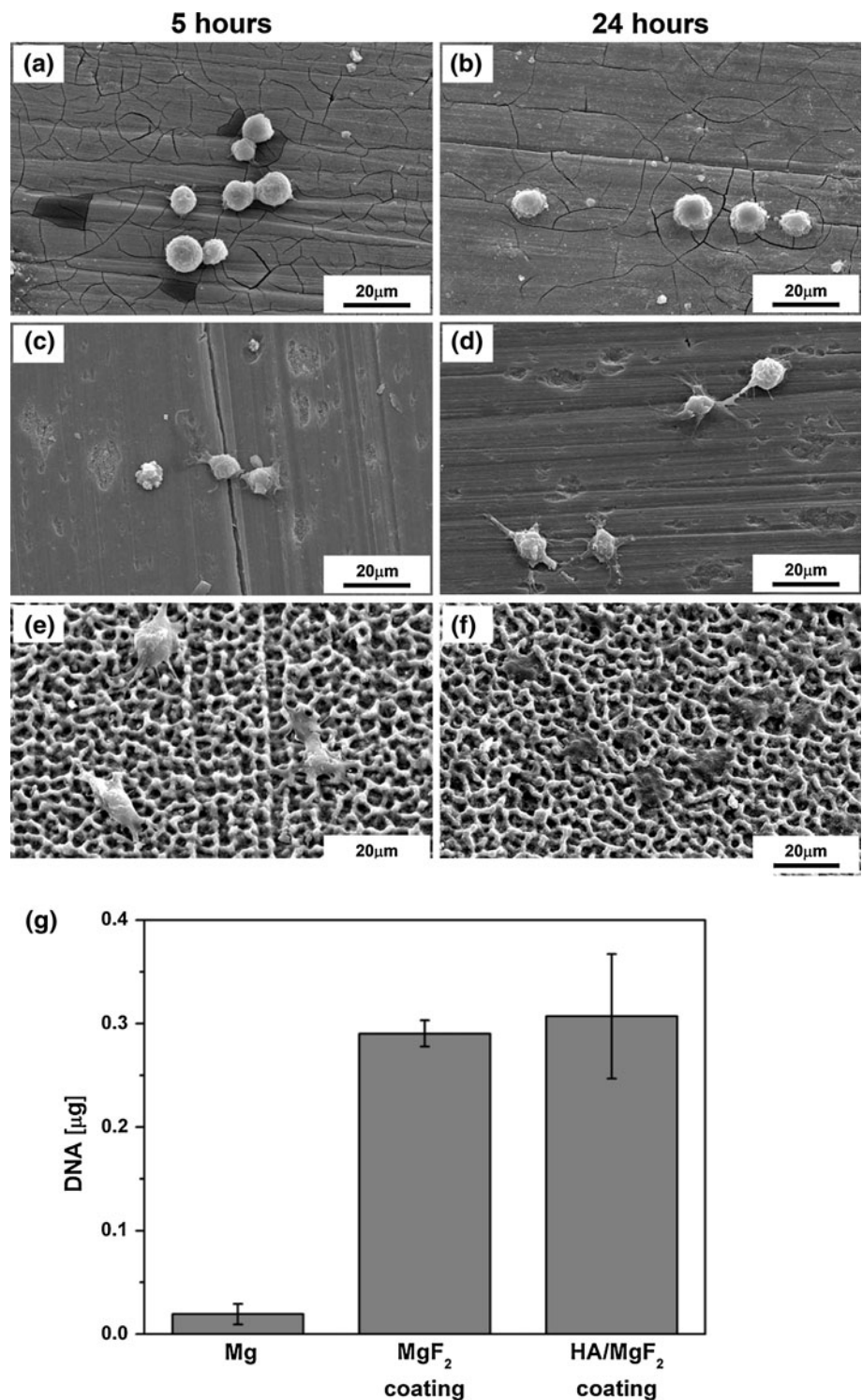
In Fig. 9, the cell proliferation was assessed by quantifying the DNA after culturing for 4 days. The cells that were cultured on the bare Mg exhibited a poor cell proliferation, whereas the proliferation levels were significantly higher on the coated Mg specimens ($P < 0.001$). The ALP activities of the cells that were cultured for up to 10 days are also shown in Fig. 9. The cells that were cultured on the HA coating layer exhibited a significantly higher ALP activity level than the bare ($P < 0.001$) and MgF₂-coated Mg ($P < 0.005$). These results clearly indicated that the HA coating improved the in vitro cellular responses of Mg and the MgF₂ coating layer.

3.5 In vivo behaviors

The in vivo behavior of the Mg implants was observed using the rabbit femoral defect model. The bare Mg and HA/MgF₂ coated Mg rod samples were implanted into the femoral shafts of the rabbits, in Fig. 10. After implantation for 4 weeks, the samples were removed, and the micro-CT images of the retrieved samples were taken in Fig. 11. The implant width of the bare Mg partially decreased because of the Mg corrosion, and a gap was clearly observed between the bone tissue and the implant in the cortical bone area. On the other hand, for the Mg specimens that were coated with HA and MgF₂, the implant shape was well maintained because of the reduced Mg corrosion, and better bone-to-implant contact was observed compared to the bare Mg.

Figure 12 illustrates the histological images of the stained bone tissue that was in contact with the implant materials. Although newly formed bone tissue was observed around the implant surface for both the bare Mg and the coated specimens, the bone contact was more significant for the coated specimens, without any implant degradation. Based

Fig. 8 Scanning electron microscopy (SEM) images of the MC3T3-E1 cells that were cultured on the **a** and **b** bare, **c** and **d** MgF₂ coated, and **e** and **f** HA/MgF₂ coated Mg samples for 5 and 24 h, respectively. **g** DNA levels that were measured from the cells that adhered to the samples after culturing for 24 h



on the histological images, the bone-to-implant contact (BIC) ratios were measured in the cortical bone area using an image analysis program, as depicted in Fig. 13. After implantation for 4 weeks, the Mg implants that were coated with HA and MgF₂ exhibited a significantly higher ($P < 0.005$) BIC ratio than the bare Mg.

4 Discussion

In recent years, various corrosion mechanisms have been identified for Mg and its alloys [7], and a great deal of research has been conducted in an attempt to control the corrosion rate of Mg so that it can be used as a degradable

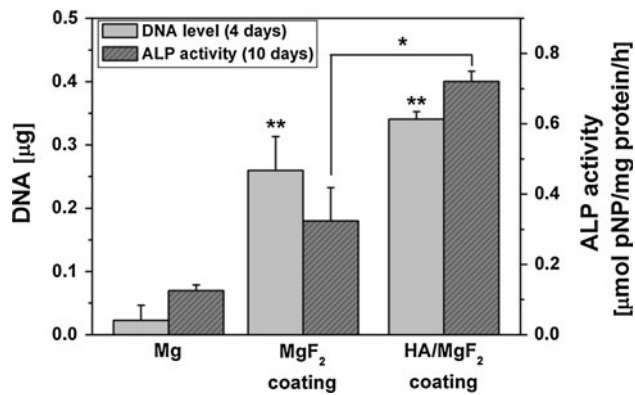


Fig. 9 DNA and ALP activity levels of the MC3T3-E1 cells that were cultured on the bare, MgF₂ coated, and HA/MgF₂ coated Mg for 4 and 10 days (* $P < 0.005$, ** $P < 0.001$)

implant material. One of the promising approaches involves coating the surfaces of Mg and its alloys. When a bioactive material is used, this surface coating can reduce the corrosion rate of Mg and improve the surface bioactivity [30]. Therefore, the selection of the proper coating material and process is crucial to the coating performance. The coating must exhibit strong adhesion to the Mg substrate, provide protection from rapid corrosion, be non-toxic, and improve the biocompatibility/bioactivity. Additionally, great care must be taken during the coating process because Mg is highly susceptible to chemical reactions. Considering these requirements, the HA coating with the MgF₂ interlayer was adopted in order to promote the coating stability on the pure Mg, while also improving both the corrosion resistance and the biocompatibility.

The HA coating with the MgF₂ interlayer was successfully and strongly adhered to Mg, in Fig. 2. These coating layers were formed without any problems during the coating process. The fluoride conversion coating process was a simple but effective technique for the protecting the substrate from corrosion, as reported in the literature [3]. A dense and crack-free ceramic HA layer was formed on the MgF₂ layer using the AD method without the need for any further heat treatment, which could provoke the oxidation of Mg. Additionally, the thickness of the coating was controllable during the AD process and influenced the HA coating degradation [37]. In this coating structure, the outer HA coating reduced the corrosion attacks, and then the MgF₂ layer protected Mg from the corrosive medium as it passed through the HA layer. Completely preventing the corrosion attack with only one coating layer is very difficult [38], and the double layer structure acted as an effective barrier for protecting Mg from corrosion. Thus, the HA coating with the MgF₂ corrosion barrier was more favorable in terms of stability and functionality on the substrate in the corrosive environment. Without the MgF₂ barrier, the HA coating layer as well as the Mg substrate

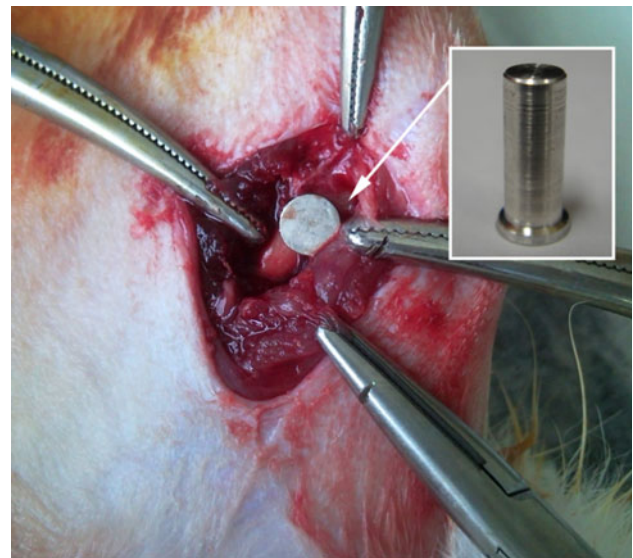


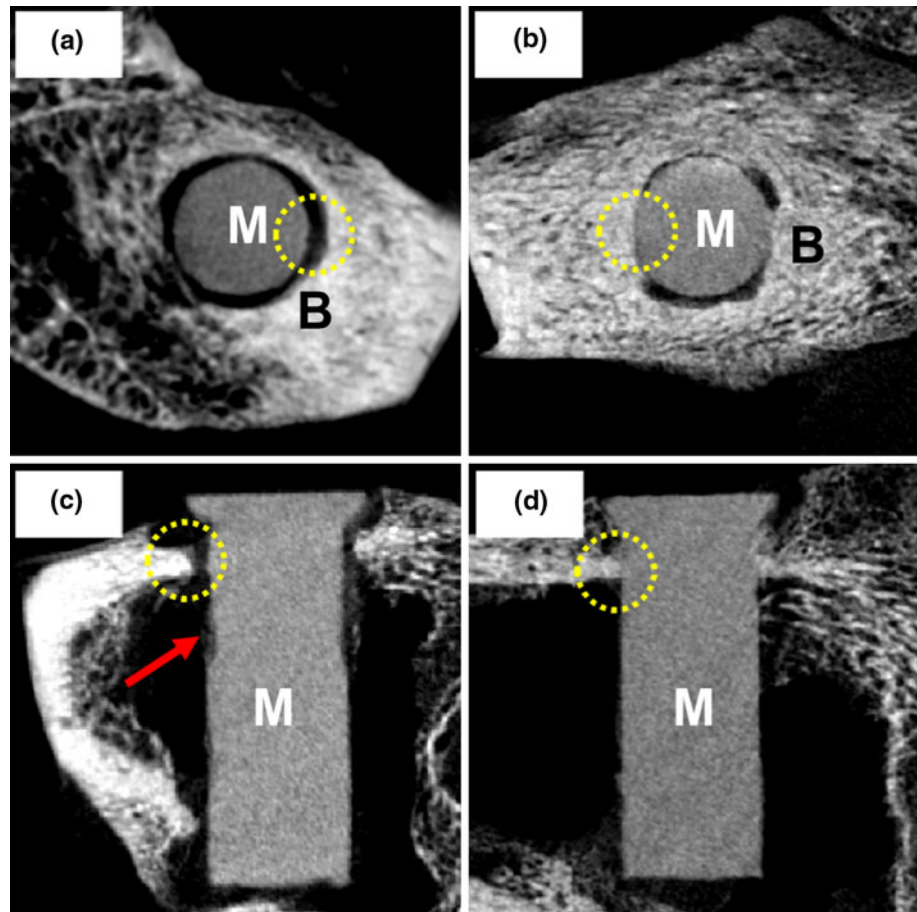
Fig. 10 Optical image of the Mg rod that was implanted into the rabbit femoral shaft. The inset shows the rod sample before the implantation

could easily be damaged by even small defects in the HA coating [39]. The HA surface coating remained stable without any severe damage during immersion in the SBF solution because of the corrosion barrier. Without the HA coating layer, the MgF₂ layer effectively protected the Mg from the corrosion attack but only for a relatively short period of time because its thickness was limited to about 1 µm. When the MgF₂ layer was thicker than 1 µm, the layer severely cracked presumably because of the large differences in the physical and mechanical properties between Mg and MgF₂.

The results of the immersion tests demonstrated that the surface coating significantly reduced the Mg corrosion in the SBF solution. The coating layers remained intact for up to 3 days, and no hydrogen bubbles were observed. Additionally, the changes in the pH and the amount of released Mg ions were insignificant compared to the bare Mg. Therefore, the hydrogen gas evolution and the alkalization, which can be detrimental to living tissue, were effectively retarded [10].

For biomedical applications, any protective coating on Mg should be non-toxic and have an improved bioactivity [4]. The in vitro cell test results revealed poor cellular responses on the bare Mg. More importantly, a much lower number of cells were observed on the bare Mg compared to the coated Mg, and the cells exhibited very slow adhesion progress. The osteoblast adhesion on material surfaces involves various biological molecules that interact together in order to induce the signal transduction and consequently regulate the subsequent cell response [40]. However, the cell adhesion processes were hindered on the bare Mg because of the corrosion reactions, resulting in the hydrogen

Fig. 11 Reconstructed micro-CT images of the **a** and **c** bare and **b** and **d** HA/MgF₂ coated Mg specimens 4 weeks after implantation. The dashed circle indicates the bone-implant contact, and the arrow indicates the corroded region (M: implant material, B: Bone tissue)



evolution and an increase in the pH. The cells exhibited better adhesion on the coated Mg, and the proliferation ($P < 0.001$) was significantly enhanced compared to the bare Mg. Moreover, the HA coating exhibited a higher ALP activity level than the bare Mg ($P < 0.001$) and the MgF₂ coating ($P < 0.005$). The cell proliferation was favorable even on the inert MgF₂ coating layer because the Mg corrosion reaction was inhibited during the cell culturing. For the cell differentiation, the bioactivity of the surface material affected the ALP activity level in addition to the corrosion protection. A large number of reports have shown that the HA coating enhances the osteoblastic cell differentiation and expresses a high ALP activity [41–43]. In this study, the HA coating with the MgF₂ interlayer significantly improved the biocompatibility of Mg.

The animal test results clearly demonstrated the positive effects of the HA coating along with the MgF₂ interlayer on the bioactivity of the Mg implant. After implantation for 4 weeks, the dimensions of the bare Mg implants changed in both the histological images and the micro-CT images. The implant thickness was partially reduced, and the original circular cross shape became irregular because of the in vivo Mg corrosion. In contrast, the morphology of the coated Mg implants was not much changed, indicating that

the coating layers were effective in protecting the implants from the in vivo corrosion. The enhanced bioactivity that was observed in the in vitro cell tests was also validated by the in vivo tests. In the 3-dimensional micro-CT images, a larger bone-implant contact area was clearly observed for the coated specimens. Furthermore, a higher BIC ratio was measured based on the histological images, thus confirming that the HA coating enhanced the bone tissue responses to the implant. The bioactive HA coating layer can also increase the bone-implant interaction and create better bone contact [43, 44]. The above in vitro and in vivo results ascertained that the HA coating with the MgF₂ interlayer significantly reduced the Mg corrosion and improved the biocompatibility. Finally, it is of note that the HA and the MgF₂ layers are not perfectly inert in the SBF solution or in animal body. They are just relatively stable compared to the Mg substrate, so that after some period of time, they are supposed to be absorbed leading to the exposure of Mg substrate. Rapid biodegradation of Mg initiates at the moment of coating layer absorption and the absorption period is proportional to the thickness of HA coating layer. Further studies are needed to verify the influence of the HA coating thickness on the Mg corrosion initiation time.

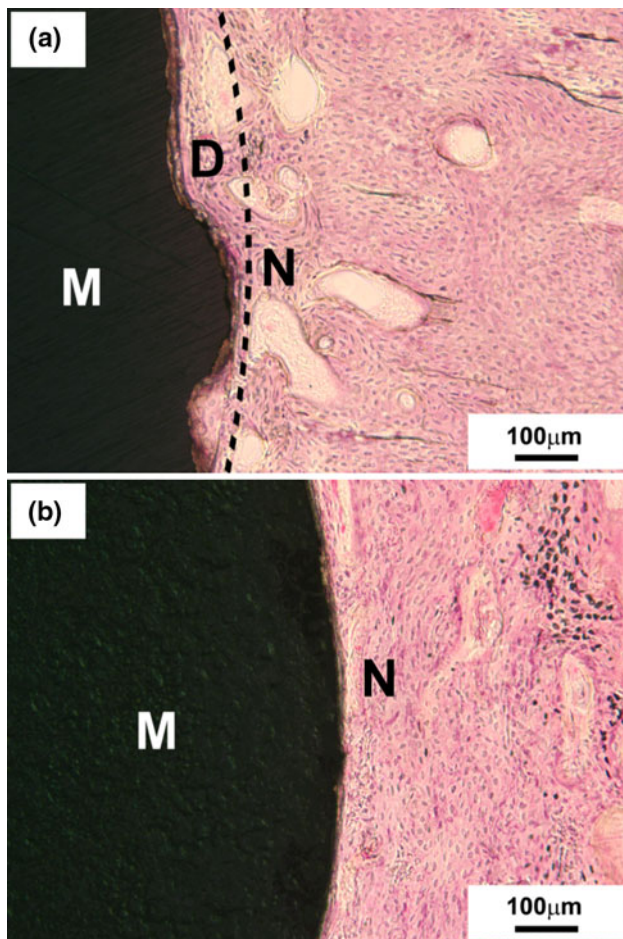


Fig. 12 Histological images of the stained sections of the **a** bare and **b** HA/MgF₂ coated Mg 4 weeks after implantation. (M: implant material; N: new bone tissue; D: degraded Mg area)

5 Conclusions

The HA coating with the MgF₂ interlayer was formed using a fluoride conversion coating technique and a subsequent aerosol deposition method. These coatings significantly improved the corrosion resistance and the bioactivity of Mg. The coating layers were uniform, dense and strongly adhered to the Mg substrate without any post treatment. The double coating layer effectively reduced the Mg corrosion rate and prevented the formation of any by-products in the SBF solution. The in vitro cell tests revealed that the coating significantly enhanced the cellular responses and the surface bioactivity. The in vivo results also demonstrated that the coating provided good in vivo corrosion protection and improved the bone responses. These results suggested that coating Mg with HA and the MgF₂ interlayer is a promising approach that increases its potential as a biodegradable implant.

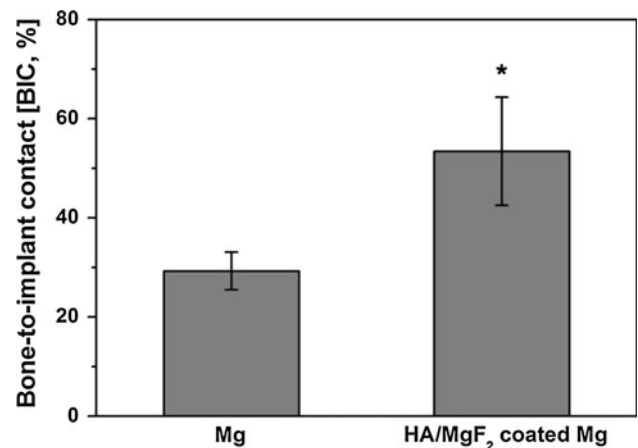


Fig. 13 Bone-to-implant contact (BIC) ratio of the bare and HA/MgF₂ coated Mg in the cortical bone area 4 weeks after implantation (* $P < 0.005$)

Acknowledgments This research was supported by WCU (World Class University) project through National Research Foundation of Korea funded by the Ministry of Education, Science and Technology (R31-2008-000-10075-0) and by the Fundamental R&D Program for Core Technology of Materials funded by the Ministry of Knowledge Economy, Republic of Korea.

References

- Nair LS, Laurencin CT. Biodegradable polymers as biomaterials. *Prog Polym Sci.* 2007;32:762–98.
- Gunatillake P, Mayadunne R, Adhikari R. Recent developments in biodegradable synthetic polymers. *Biotechnol Annu Rev.* 2006;12:301–47.
- Chiu KY, Wong MH, Cheng FT, Man HC. Characterization and corrosion studies of fluoride conversion coating on degradable Mg implants. *Surf Coat Tech.* 2007;202:590–8.
- Staiger MP, Pietak AM, Huadmai J, Dias G. Magnesium and its alloys as orthopedic biomaterials: a review. *Biomaterials.* 2006; 27:1728–34.
- Zreiqat H, Howlett CR, Zannettino A, Evans P, Schulze-Tanzil G, Knabe C, et al. Mechanisms of magnesium-stimulated adhesion of osteoblastic cells to commonly used orthopaedic implants. *J Biomed Mater Res.* 2002;62:175–84.
- Zeng RC, Dietzel W, Witte F, Hort N, Blawert C. Progress and challenge for magnesium alloys as biomaterials. *Adv Eng Mater.* 2008;10:B3–14.
- Song GL, Atrens A. Corrosion mechanisms of magnesium alloys. *Adv Eng Mater.* 1999;1:11–33.
- Witte F, Kaese V, Haferkamp H, Switzer E, Meyer-Lindenberg A, Wirth CJ, et al. In vivo corrosion of four magnesium alloys and the associated bone response. *Biomaterials.* 2005;26: 3557–63.
- Witte F, Fischer J, Nellesen J, Crostack HA, Kaese V, Pisch A, et al. In vitro and in vivo corrosion measurements of magnesium alloys. *Biomaterials.* 2006;27:1013–8.
- Song GL. Control of biodegradation of biocompatible magnesium alloys. *Corros Sci.* 2007;49:1696–701.
- Wang H, Estrin Y, Fu H, Song G, Zuberova Z. The effect of pre-processing and grain structure on the bio-corrosion and fatigue

- resistance of magnesium alloy AZ31. *Adv Eng Mater.* 2007;9:967–72.
12. Xu LP, Yu GN, Zhang E, Pan F, Yang K. In vivo corrosion behavior of Mg-Mn-Zn alloy for bone implant application. *J Biomed Mater Res A.* 2007;83A:703–11.
 13. Li ZJ, Gu XN, Lou SQ, Zheng YF. The development of binary Mg-Ca alloys for use as biodegradable materials within bone. *Biomaterials.* 2008;29:1329–44.
 14. Pietak A, Mahoney P, Dias GJ, Staiger MP. Bone-like matrix formation on magnesium and magnesium alloys. *J Mater Sci-Mater M.* 2008;19:407–15.
 15. Kannan MB, Raman RKS. In vitro degradation and mechanical integrity of calcium-containing magnesium alloys in modified-simulated body fluid. *Biomaterials.* 2008;29:2306–14.
 16. Xu LP, Zhang EL, Yin DS, Zeng SY, Yang K. In vitro corrosion behaviour of Mg alloys in a phosphate buffered solution for bone implant application. *J Mater Sci-Mater M.* 2008;19:1017–25.
 17. Gu XN, Zheng YF, Cheng Y, Zhong SP, Xi TF. In vitro corrosion and biocompatibility of binary magnesium alloys. *Biomaterials.* 2009;30:484–98.
 18. Hanzi AC, Gunde P, Schinhammer M, Uggowitzer PJ. On the biodegradation performance of an Mg-Y-RE alloy with various surface conditions in simulated body fluid. *Acta Biomater.* 2009;5:162–71.
 19. Zhang EL, Xu LP, Yu GN, Pan F, Yang K. In vivo evaluation of biodegradable magnesium alloy bone implant in the first 6 months implantation. *J Biomed Mater Res A.* 2009;90A:882–93.
 20. Witte F, Hort N, Vogt C, Cohen S, Kainer KU, Willumeit R, et al. Degradable biomaterials based on magnesium corrosion. *Curr Opin Solid St M.* 2008;12:63–72.
 21. Song GL, Song SZ. A possible biodegradable magnesium implant material. *Adv Eng Mater.* 2007;9:298–302.
 22. Song YW, Shan DY, Han EH. Electrodeposition of hydroxyapatite coating on AZ91D magnesium alloy for biomaterial application. *Mater Lett.* 2008;62:3276–9.
 23. Xu LP, Zhang EL, Yang K. Phosphating treatment and corrosion properties of Mg-Mn-Zn alloy for biomedical application. *J Mater Sci-Mater M.* 2009;20:859–67.
 24. Zhang E, Xu LP, Yang K. Formation by ion plating of Ti-coating on pure Mg for biomedical applications. *Scripta Mater.* 2005;53:523–7.
 25. Gray-Munro JE, Seguin C, Strong M. Influence of surface modification on the in vitro corrosion rate of magnesium alloy AZ31. *J Biomed Mater Res A.* 2009;91A:221–30.
 26. Wen CL, Guan SK, Peng L, Ren CX, Wang X, Hu ZH. Characterization and degradation behavior of AZ31 alloy surface modified by bone-like hydroxyapatite for implant applications. *Appl Surf Sci.* 2009;255:6433–8.
 27. Geng F, Tan LL, Jin XX, Yang JY, Yang K. The preparation, cytocompatibility, and in vitro biodegradation study of pure beta-TCP on magnesium. *J Mater Sci-Mater M.* 2009;20:1149–57.
 28. Zhang YJ, Zhang GZ, Wei M. Controlling the biodegradation rate of magnesium using biomimetic apatite coating. *J Biomed Mater Res B.* 2009;89B:408–14.
 29. Wang Y, Wei M, Gao JC. Improve corrosion resistance of magnesium in simulated body fluid by dicalcium phosphate dihydrate coating. *Mat Sci Eng C-Bio S.* 2009;29:1311–6.
 30. Xu LP, Pan F, Yu GN, Yang L, Zhang EL, Yang K. In vitro and in vivo evaluation of the surface bioactivity of a calcium phosphate coated magnesium alloy. *Biomaterials.* 2009;30:1512–23.
 31. Lakstein D, Kopelovitch W, Barkay Z, Bahaa M, Hendel D, Eliaz N. Enhanced osseointegration of grit-blasted, NaOH-treated and electrochemically hydroxyapatite-coated Ti-6Al-4V implants in rabbits. *Acta Biomater.* 2009;5:2258–69.
 32. Bigi A, Fini M, Bracci B, Boanini E, Torricelli P, GiavareSi G, et al. The response of bone to nanocrystalline hydroxyapatite-coated Ti13Nb11Zr alloy in an animal model. *Biomaterials.* 2008;29:1730–6.
 33. Akedo J. Aerosol deposition of ceramic thick films at room temperature: densification mechanism of ceramic layers. *J Am Ceram Soc.* 2006;89:1834–9.
 34. Hahn BD, Park DS, Choi JJ, Ryu J, Yoon WH, Kim KH, et al. Dense nanostructured hydroxyapatite coating on titanium by aerosol deposition. *J Am Ceram Soc.* 2009;92:683–7.
 35. Kokubo T, Takadama H. How useful is SBF in predicting in vivo bone bioactivity? *Biomaterials.* 2006;27:2907–15.
 36. Hahn BD, Lee JM, Park DS, Choi JJ, Ryu J, Yoon WH, et al. Aerosol deposition of silicon-substituted hydroxyapatite coatings for biomedical applications. *Thin Solid Films.* 2010;518:2194–9.
 37. Gineste L, Gineste M, Ranz X, Ellefterion A, Guilhem A, Rouquet N, et al. Degradation of hydroxyapatite, fluorapatite, and fluorhydroxyapatite coatings of dental implants in dogs. *J Biomed Mater Res.* 1999;48:224–34.
 38. Guo XX, Xu SL, Zhao LL, Lu W, Zhang FZ, Evans DG, et al. One-step hydrothermal crystallization of a layered double hydroxide/alumina bilayer film on aluminum and its corrosion resistance properties. *Langmuir.* 2009;25:9894–7.
 39. Dearnley PA. A brief review of test methodologies for surface-engineered biomedical implant alloys. *Surf Coat Tech.* 2005;198:483–90.
 40. Meyer U, Buchter A, Wiesmann HP, Joos U, Jones DB. Basic reactions of osteoblasts on structured material surfaces. *Eur Cell Mater.* 2005;9:39–49.
 41. Kim HW, Koh YH, Li LH, Lee S, Kim HE. Hydroxyapatite coating on titanium substrate with Titania buffer layer processed by sol-gel method. *Biomaterials.* 2004;25:2533–8.
 42. Hahn BD, Lee JM, Park DS, Choi JJ, Ryu J, Yoon WH, et al. Mechanical and in vitro biological performances of hydroxyapatite-carbon nanotube composite coatings deposited on Ti by aerosol deposition. *Acta Biomater.* 2009;5:3205–14.
 43. Ramires PA, Wennerberg A, Johansson CB, Cosentino F, Tundo S, Milella E. Biological behavior of sol-gel coated dental implants. *J Mater Sci-Mater M.* 2003;14:539–45.
 44. Faeda RS, Tavares HS, Sartori R, Guastaldi AC, Marcantonio E. Biological performance of chemical hydroxyapatite coating associated with implant surface modification by laser beam: biomechanical study in rabbit tibias. *J Oral Maxil Surg.* 2009;67:1706–15.